

# Simultaneous X-ray and radio observations of Young Stellar Objects in NGC 1333 and IC 348

Jan Forbrich<sup>1</sup>, Rachel Osten<sup>2</sup>, & Scott J. Wolk<sup>1</sup>

## ABSTRACT

Young Stellar Objects (YSOs) and in particular protostars are known to show a variety of high-energy processes. Observations in the X-ray and centimetric radio wavelength ranges are thought to constrain some of these processes, e.g., coronal-type magnetic activity. There is a well-known empirical correlation of radio and X-ray luminosities in active stars, the so-called Güdel-Benz relation. Previous evidence whether YSOs are compatible with this relation remains inconclusive for the earliest evolutionary stages. The main difficulty is that due to the extreme variability of these sources, simultaneous observations are essential. Until now, only few YSOs and only a handful of protostars have been observed simultaneously in the X-ray and radio range. To expand the sample, we have obtained such observations of two young clusters rich in protostars, NGC 1333 and IC 348. While the absolute sensitivity is lower for these regions than for more nearby clusters like CrA, we find that even in deep continuum observations carried out with the NRAO Very Large Array, the radio detection fraction for protostars in these clusters is much lower than the X-ray detection fraction. Very few YSOs are detected in both bands, and we find the radio and X-ray populations among YSOs to be largely distinct. We combine these new results with previous simultaneous *Chandra* and VLA observations of star-forming regions and find that YSOs with detections in both bands appear to be offset toward higher radio luminosities for given X-ray luminosities when compared to the Güdel-Benz relation, although even in this sensitive dataset most sources are too weak for the radio detections to provide information on the emission processes. The considerably improved sensitivity of the Expanded Very Large Array will provide a better census of the YSO radio population as well as better constraints on the emission mechanisms.

*Subject headings:* stars: protostars – stars: pre-main sequence – radio continuum: stars – X-rays: stars

## 1. Introduction

Young Stellar Objects (YSOs) have been known for some time to be observable in X-ray and radio emission, tracers of high-energy processes (e.g., Feigelson & Montmerle 1999). Briefly, thermal X-ray emission is thought to be produced by hot plasma heated in coronal-type activity while non-thermal radio emission traces magnetic fields that may be cospatial to and confining the X-ray emitting plasma. YSOs are typically grouped

into classes, starting with class 0/I protostars as the earliest stages, and progressing through disk-dominated class II objects to basically diskless class III sources, also known as weak-line T Tauri stars. These objects are progressively less embedded, and the importance of first the protostellar envelope and then the protostellar disks diminishes (Lada 1987; André et al. 1993).

There are several effects which complicate a direct comparison of the high-energy processes of YSOs and solar-like stars. Circumstellar disks, a defining characteristic of protostars, may affect the overall shape of the magnetic field, for example by providing support for large magnetic structures connecting the central object and the

<sup>1</sup>Harvard-Smithsonian Center for Astrophysics, 60 Garden Street, Cambridge, MA 02138, USA

<sup>2</sup>Space Telescope Science Institute, 3700 San Martin Drive, Baltimore, MD 21218, USA

disk. Radio emission may be dominated by either nonthermal emission originating in magnetic fields, or thermal emission from the disk or stellar wind. The latter is usually interpreted as thermal bremsstrahlung due to ionized material while the former most frequently is (gyro)synchrotron radiation (e.g., Dulk 1985; André 1996; Güdel 2002). Note that thermal emission can easily conceal non-thermal emission from underneath due to its optical depth. André (1987) estimate that a spherical ionized stellar wind of only a few  $10^{-11} M_{\odot} \text{ yr}^{-1}$  is already opaque. While it may thus seem unlikely that there is a chance to detect any nonthermal emission from protostars at all, such cases have been reported (Feigelson et al. 1998; Shirley et al. 2007).

There are a few different methods to identify nonthermal radio sources in contrast to thermal sources. The two primary indications are polarization and negative spectral indices, as derived from the two simultaneously measured radio bands. Here, the spectral index  $\alpha$  is defined as  $S_{\nu} \propto \nu^{\alpha}$ , and a negative spectral index  $\alpha < -0.1$  is an indication of optically thin nonthermal emission (e.g., André 1996). While a two-frequency spectral index is not a very reliable indicator, the detection of polarized emission is the most unambiguous sign of non-thermal emission as observed with the VLA. However, due to the small degree of polarization (e.g., White et al. 1992; Feigelson et al. 1998), high S/N ratios are required to meaningfully detect or constrain such polarization. A third indication is the existence of short-term variability.

While it is not obvious that thermal hot-plasma X-ray emission and nonthermal radio emission should have an observable underlying connection, certain types of solar flares and a variety of active stars have been shown to have correlated X-ray and (nonthermal) radio luminosities according to the so-called Güdel-Benz (GB) relation,  $L_X/L_R \approx 10^{15 \pm 1} \text{ Hz}$ , extending over 10 orders of magnitude (Güdel & Benz 1993; Benz & Güdel 1994; Güdel 2002). The explanation which these authors suggested for the nearly linear correlation between X-ray and radio luminosities relied on a common energy reservoir for both plasma heating and particle acceleration, and a similar partitioning of energy into these two processes over 10 orders of magnitude in stellar luminosity. For a

recent summary of the X-ray–radio correlation in cool stars, see Forbrich et al. (2011).

The early studies on correlated X-ray and radio luminosities of different object classes included some weak-line T Tauri stars (class III sources) as powerful radio and X-ray sources, even though the underlying observations were non-simultaneous. It is therefore interesting to find out whether YSOs in earlier evolutionary stages, particularly class I protostars – strong X-ray and radio sources in their own right – are compatible with the GB relation. Since YSOs are highly variable, this question is preferably addressed by simultaneous X-ray and radio observations. Until now, there have been few such observations of YSOs. V773 Tau, a T Tauri star, became the first YSO observed in this way, and radio variability exceeding the X-ray variability was found (Feigelson et al. 1994; Guenther et al. 2000). Bower et al. (2003) reported the serendipitous simultaneous radio and X-ray observation of a spectacular radio flare toward a weak-line T Tauri star in Orion (GMR-A). In the first study targeting a subset of an entire star-forming region, Gagné et al. (2004) observed the  $\rho$  Oph cloud complex with *Chandra* and the NRAO Very Large Array. Several T Tauri stars were detected in both wavelength ranges, but no clear X-ray–radio correlation was found. Subsequently, Forbrich et al. (2007) succeeded in detecting several class I protostars in the CrA star-forming region simultaneously in the X-ray and radio wavelength ranges. Among the YSOs in CrA detected in both bands, most are compatible with the GB relation. Most recently, Osten & Wolk (2009) report the detections in both bands of several T Tauri stars in the LkH $\alpha$  101 cluster. Here, no clear X-ray–radio correlation was found.

In an attempt to observe more protostars simultaneously in the X-ray and radio wavelength ranges, we have observed selected regions in two more young clusters, IC 348 and NGC 1333. Previously published observations carried out with the *Spitzer Space Telescope* serve as an excellent road map to locate YSOs in early evolutionary stages in these clusters. Two-frequency radio observations help us in potentially discriminating between nonthermal and thermal radio sources, based on the value of the radio spectral indices. We will discuss the results in the context of previous simultaneous radio and X-ray observations of

YSOs.

### 1.1. The target regions: IC 348 and NGC 1333

Located in the Perseus Molecular Cloud, both IC 348 and NGC 1333 are prominent nearby star-forming regions (for recent reviews, see Herbst 2008 and Walawender et al. 2008, respectively, and Bally et al. 2008). The most accurate distance has been determined toward NGC 1333 by measuring the parallax of the bright maser source SVS 13 (Hirota et al. 2008), yielding  $235 \pm 18$  pc. IC 348 is slightly more distant at about 260 pc (Lombardi et al. 2010). The star formation activity in both regions has been surveyed extensively. Most relevant for our purposes are studies using the *Spitzer Space Telescope* to identify and classify YSOs in early evolutionary stages by their infrared excess emission. Lada et al. (2006) analyzed  $\sim 300$  previously known members of IC 348 and classified them by their disk properties, distinguishing stellar (photospheric), anemic, and thick-disk spectral energy distributions (SEDs). The main basis for this classification is the dereddened *Spitzer*-IRAC slope. In a follow-up paper, Muench et al. (2007) identified and analyzed new cluster members, including embedded class I protostars. Their class II category corresponds to the thick disks from Lada et al., even though the spectral indices of some thick disk sources from Lada et al. (2006) qualify as class I sources according to Muench et al. (2007). To use a consistent classification, we follow the spectral index limits in Muench et al. (2007) without separating out flat-spectrum sources. The class III objects in Muench et al. (2007) correspond to the anemic and photospheric sources in Lada et al. (2006). The NGC 1333 region was similarly surveyed by Gutermuth et al. (2008) who employ a three-phase technique to identify YSOs. Our focus here is on the youngest evolutionary stages. This is due both to scientific interest and the fact that in both regions previous surveys have been most complete for class I and class II sources. However, our study also reveals class III sources. Since the *Spitzer* studies cannot distinguish class 0 and class I sources, we additionally use the sources identified by Enoch et al. (2009) in Perseus to find the class 0 sources among the *Spitzer* class I sources. Compared to star-forming regions that have previously

been targets of simultaneous X-ray and radio observations (see above), IC 348 and NGC 1333 are about twice as distant as Taurus,  $\rho$  Oph, and CrA, but at less than half the distance of LkH $\alpha$  101.

### 1.2. Previous radio observations

Both IC 348 and NGC 1333 have been observed with the NRAO<sup>1</sup> Very Large Array (VLA) prior to our own observations. Our region of interest in IC 348 has been observed by Avila et al. (2001) who present a deep radio dataset centered on HH 211. Their concatenated dataset has a quoted rms noise sensitivity of  $12 \mu\text{Jy}$  and consists of a short C array observation obtained in 1994 and 9.7 h of on-source time using 11 VLA antennas in 1999. The phase center of these observations lies  $\sim 9'$  off our position 1 (see below) and  $\sim 2'$  off our position 2.

NGC 1333 was studied in VLA observations of SVS 13 and its surroundings. After an initial study (Rodríguez et al. 1997) with two observations reaching sensitivities of  $30 \mu\text{Jy}$  and  $20 \mu\text{Jy}$ , deep concatenated archival datasets in the 3.6 cm (X) and 6 cm bands (C) were presented by (Rodríguez et al. 1999). While these datasets contain data obtained in various configurations, a common subset of the  $uv$  plane has been used for the combined data, resulting in angular resolutions of  $4''$ – $5''$  in both bands. The phase centers of these observations coincide with our southern pointing (see below) whereas our northern pointing is off by  $\sim 7'$ .

## 2. Observations and data analysis

Both IC 348 and NGC 1333 have been observed with very similar observational setups. Since the *Chandra*-ACIS field of view ( $17' \times 17'$ ) is considerably larger than the VLA primary beam, we have selected two VLA pointings within the *Chandra* fields (see Figure 1). Using the VLA with two distinct subarrays allows us to record two different radio frequencies simultaneously.

---

<sup>1</sup>The National Radio Astronomy Observatory is a facility of the National Science Foundation operated under cooperative agreement by Associated Universities, Inc.

## 2.1. IC 348

A region centered on RA 03h43m59.90s, Dec +31°58'21.70" was observed with *Chandra* ACIS-I in two 40 ksec observations on March 13 and on March 18, 2008 (IDs 8933 and 8944). Simultaneous radio observations were carried out with the VLA in its C configuration (project ID S9056). Two subarrays were used to cover the X and C bands simultaneously, using 13 antennas in X band and 14 antennas in C band. Two pointing positions within the ACIS-I field of view were observed alternately, RA 03h44m13.58s, Dec +32°00'24.21" (position 1) and RA 03h43m52.96s, Dec +32°02'44.21" (position 2). Total on-source time for each pointing and frequency is approximately 10.0 hours. The full-width half-maximum primary beam sizes in the X and C bands are 5.3' and 9.6', respectively. An absolute flux density scale was established by an observation of 3C147 on the second day of observations. The phase calibrator 0336+323 was observed after each 20 min scan on one of the two pointing positions. The primary calibrator (3C147) was at 4.68 Jy (X-band) and 7.86 Jy (C-band), and the phase calibrator 0336+323 had bootstrapped flux densities of 1.24 Jy (X-band) and 1.68 Jy (C-band).

## 2.2. NGC 1333

A region centered on RA 03h29m02.00s, Dec +31°20'54.00" was observed with *Chandra* ACIS-I in two 40 ksec observations on July 5 and on July 11, 2006 (IDs 6436 and 6437). Simultaneous radio observations were carried out with the NRAO Very Large Array (VLA) in its B configuration (project ID S7874). Two subarrays with 13 antennas each were used to cover the X and C bands simultaneously. Two pointing positions within the ACIS-I field of view were observed alternately, RA 03h29m14.072s, Dec +31°22'40.06" (position N) and RA 03h29m04.941s, Dec +31°15'54.37" (position S). The total on-source time for each pointing and frequency is approximately 9.4 hours and the typical on-source scan-duration was 15 minutes. An absolute flux density scale was established by observations of 3C286 on both days of observations. The phase calibrator 0336+323, the same that was also used for IC 348, was observed after each scan on one of the two pointing positions. The primary calibrator (3C286) was

at 5.20 Jy (X-band) and 7.49 (C-band), and the phase calibrator 0336+323 had bootstrapped flux densities of 1.91 Jy (X-band) and 2.28 Jy (C-band).

## 2.3. Sensitivity

Given the different sizes of the fields of view of *Chandra*-ACIS and the VLA, there is a trade-off between increasing spatial coverage by using several VLA pointings and increasing sensitivity by observing only one position. Additionally, observations at only one frequency would be more sensitive than the use of two frequencies, either by using two subarrays or by observing separately. As a compromise, we opted for a setup using two pointings and two frequency bands: a loss of sensitivity. Compared to a setup where we would maximize sensitivity by observing a single position with all antennas at one frequency, we lose a factor of  $2\cdot\sqrt{2}=2.8$  in flux density sensitivity. Primarily due to the different distances to star-forming regions, this study is not as sensitive as the  $\rho$  Oph study by Gagné et al. (2004) or the CrA study by Forbrich et al. (2007). Our observation strategy is a compromise between the one employed by Gagné et al. (2004) who used a mosaic of VLA pointings to cover the *Chandra* field and Forbrich et al. (2006) who maximized sensitivity by using only one pointing position and frequency. We show a more detailed comparison of the various simultaneous *Chandra* and VLA observations of star-forming regions in Table 1.

## 2.4. Data reduction and analysis

All VLA observations were analyzed using the NRAO Astronomical Image Processing System (AIPS), following standard procedure. After data flagging and calibration, the primary beam areas of both experiments were imaged using a robustness power of 0 for *uv* weighting as a compromise between sensitivity and synthesized beam size. For the best sensitivity in subsequent source detection both observing epochs of the two clusters were combined for imaging. Source detection was performed using the AIPS task 'SAD' above a S/N ratio of 5. All maps have rms noise levels near the theoretical expectation of  $18 \mu\text{Jy}$ , based on the VLA Exposure Calculator<sup>2</sup>, assuming 10 hours of

<sup>2</sup><http://www.vla.nrao.edu/astro/guides/exposure/calc.html>

TABLE 1  
SENSITIVITIES OF SIMULTANEOUS *Chandra* AND VLA OBSERVATIONS OF STAR-FORMING REGIONS

Target	Date	$d$ (pc)	$L_R(5\sigma)$ ( $\text{erg s}^{-1} \text{Hz}^{-1}$ )	$L_X(5 \text{ cnts})$ ( $\text{erg s}^{-1}$ )	References
$\rho$ Oph	May 2000	130 <sup>a</sup>	$3.2 \times 10^{15}$	$7.8 \times 10^{26}$	Gagné et al. (2004)
LkHa101	Mar 2005	510	$1.5 \times 10^{16}$	$1.5 \times 10^{28}$	Osten & Wolk (2009)
CrA	Aug 2005	130	$1.7 \times 10^{15}$	$1.0 \times 10^{27}$	Forbrich et al. (2007) <sup>b</sup>
NGC 1333	Jul 2006	235	$6.9 \times 10^{15}$	$3.2 \times 10^{27}$	this work
IC 348	Mar 2008	250	$5.7 \times 10^{15}$	$3.6 \times 10^{27}$	this work

NOTE.—The radio and X-ray sensitivities have been determined using the  $5\sigma$  radio detection limit in either C or X band and assuming a 5 count detection limit of an unabsorbed source with an APEC hot-plasma spectrum (with a temperature of 1 keV) in the *Chandra* data, as determined using PIMMS (Mukai 1993).

<sup>a</sup>Gagné et al. (2004) assume  $d = 165$  pc, but see discussion in Wilking et al. (2008).

<sup>b</sup>From simultaneous observations. For deeper radio and X-ray data, see Forbrich et al. (2006) and Forbrich & Preibisch (2007).

on-source time at full bandwidth, effectively 86 MHz, and 13 antennas. The fitted source flux densities were corrected for primary beam attenuation and the peak flux densities from the fits are reported in the tables. Radio upper limits were determined on maps that were previously corrected for primary-beam attenuation. The synthesized beam sizes are on the order of  $2.5''$  (IC 348) and  $0.8''$  (NGC 1333) in X band and on the order of  $4.0''$  (IC 348) and  $1.2''$  (NGC 1333) in C band.

The *Chandra* X-ray observations have been reduced using the ANCHORS pipeline (AN archive of Chandra Observations of Regions of Star formation<sup>3</sup>). The X-ray observations of NGC 1333 have already been published elsewhere (Winston et al. 2010). Full details of the ANCHORS processing are also given there. For previous X-ray results on NGC 1333, see also Getman et al. (2002).

<sup>3</sup><http://cxc.harvard.edu/ANCHORS>

### 3. Results

#### 3.1. Radio data

##### 3.1.1. IC 348

Only five radio sources were detected in the two integrated IC 348 pointings above a significance of  $5\sigma$  (map rms  $14 \mu\text{Jy}$ ). In addition to using the AIPS task SAD, we have manually searched about 160 YSO positions reported by Lada et al. (2006) and Muench et al. (2007) for lower-significance detections in either the X or C-bands, if they were reasonably close to the pointing centers. This search resulted in two additional detections, VLA 2 and LRL 51. While VLA 2 has been reported as a radio source before, LRL 51 has not. Since LRL 51 is detected in both radio bands, it seems unlikely that this would be due to a chance alignment with a noise peak; see the discussion of chance alignments for NGC 1333 below.

In Table 2, we list the total of seven radio detections in the nominal primary beam areas (FWHM) from both detection methods. Five sources can be identified with sources from the samples of Lada et al. (2006) and Muench et al. (2007). These are HH 211-mm, a class 0 proto-

star, LRL 52590 and LRL 51, class I sources, LRL 13 (class II), as well as LRL 49, a source listed as having a stellar SED (class III). Additionally, we note weak outflow-like emission on opposing sides of LRL 54459/54460 and LRL 57025, but these tentative detections are not listed in the source table. Source 7 does not have infrared or optical counterparts; it is thus probably extragalactic.

To identify signs of nonthermal emission, we have also searched Stokes- $V$  maps for detections of circularly polarized sources, a telltale sign for gyrosynchrotron radiation. No sources were detected above  $5\sigma$  in a Stokes- $V$  map; the  $3\sigma$  upper limits for the two brightest YSOs are  $45 \mu\text{Jy}$ , corresponding to upper limits for the circular polarization of LRL 52590 and LRL 49 of 3.5% and 8.2%. Additionally, we are particularly interested in radio counterparts with negative spectral indices, again indicative of nonthermal emission. However, we do not find clear cases of negative spectral indices. While LRL 13 only has a C band counterpart and remains undetected in the X band, the detection is too weak for the upper limit of the spectral index to be significant.

The low number of detections correspond to low detection rates since considerably more YSOs are located in the primary beam areas. Table 3 lists the different source types located in the primary beam areas of the X-band and C-band observations as well as the respective radio detections. As noted above, the C-band primary beam is larger than the X-band primary beam. All YSO classes have very low detection rates. Overall, only 10% of the class 0-II YSOs in the C-band primary beam areas were detected.

Our list of detections contains two of the four sources reported by Avila et al. (2001) in a deeper observation. For the two undetected sources, we can report upper limits. VLA 1 was reported with an X-band flux density of 0.14 mJy where we find an upper limit of  $< 0.07$  mJy ( $5\sigma$ ), and for VLA 4, the reported X-band flux density of 0.59 mJy compares to our upper limit of  $< 0.08$  mJy ( $5\sigma$ ). These two sources appear to have no known counterparts at other wavelengths and probably are variable extragalactic radio sources. Both VLA 2 and VLA 3 also show variability on the time scales of years. VLA 2 is slightly weaker, but statistically marginally compatible with the previous result while VLA 3 has become brighter. We sum-

marize this comparison in Table 4. Among our radio detections, only one source is located in the primary beam area of the Avila et al. (2001) observations, i.e., source 4, or LRL 13. However, we only detect the source in C band while Avila et al. (2001) only discuss X band data.

When imaging the two epochs of this experiment separately, some variability on time scales of days becomes apparent. Only two of the sources seen in the full dataset are detected at  $> 5\sigma$  in the single epochs and are listed in Table 5. Interestingly, we also detect and list two more sources that are detected above the same threshold in only one of the two epochs and remain below the  $5\sigma$  cutoff in the combined data (note that these are not included in Table 3). One is LRL 1888, listed by Muench et al. (2007) as a candidate class III member, and the other is unidentified, though within  $1''$  of a previously listed infrared source ([PSZ2003] J034403.6+320520). Both detections are too weak for reliable determinations of spectral indices.

### 3.1.2. NGC 1333

We have used the same methods that were used for IC 348 for source detection in NGC 1333. An automatic search above a significance cutoff of  $5\sigma$  was followed by a manual search for lower-significance detections toward previously reported radio sources (Rodríguez et al. 1999) and YSOs (Gutermuth et al. 2008); the typical map rms is  $20 \mu\text{Jy}$ . Nine sources were detected by the automatic search while ten more sources were found manually. The resulting source list with 19 sources is shown in Table 6.

At detection significance levels of  $3\sigma$ , used in the manual search, the number of false detections due to noise peaks is no longer negligible. When using the total number of sources that we searched manually and assuming Gaussian noise, we expect  $\sim 1-3$  false detections in the X and C bands due to chance alignments of candidate sources and positive image pixels with  $> 3\sigma$  significance within the area of a synthesized beam. Note that this only holds for detections in just one of the two bands. While Table 6 also contains sources with single-band detections at levels of  $< 5\sigma$ , these could thus be chance alignments.

In addition to such alignments with noise peaks, there are also detections of extragalactic sources in

TABLE 2  
IC 348: RADIO DETECTIONS

no.	Pos	RA, Dec (J2000.0)	$S_X$ (mJy)	$S_C$ (mJy)	$\alpha$ (X-C)	ID (lit.)
1	2	3:43:56.816 +32:00:50.06	$0.087 \pm 0.022$	$0.040 \pm 0.016$		VLA 2, HH 211-mm (0)
2	2	3:43:57.099 +32:03:03.79	$0.079 \pm 0.015$	$< 0.07$ ( $5\sigma$ )		
3	2	3:43:57.610 +32:01:37.39	$0.552 \pm 0.017$	$0.542 \pm 0.015$	$0.03 \pm 0.11$	VLA 3, LRL 49 (STAR)
4	2	3:43:59.707 +32:01:53.43	$< 0.08$ ( $5\sigma$ )	$0.087 \pm 0.014$		LRL 13 (THICK,II)
5	1	3:44:12.990 +32:01:35.71	$0.057 \pm 0.018$	$0.054 \pm 0.017$		LRL 51 (THICK,I)
6	1	3:44:20.377 +32:01:58.60	$1.312 \pm 0.021$	$1.146 \pm 0.019$	$0.25 \pm 0.06$	LRL 52590 (I)
7	1	3:44:31.459 +32:00:39.96	out of pb	$0.227 \pm 0.026$	–	no IR counterpart

NOTE.—The spectral index is only given when the corresponding error is  $\leq 0.2$ . The second column refers to a detection in either of the two pointings, as defined in the text. The VLA designations are from Avila et al. (2001) and the LRL numbers and classifications are from Lada et al. (2006) and Muench et al. (2007). The two thick disk sources from Lada et al. (2006) have different classes according to the spectral index criterion used by Muench et al. (2007). For HH 211-mm, see Froebrich et al. (2003).

TABLE 3  
IC 348: RADIO – DETECTED MEMBERS

	FOV (C)	FOV (X)	det. in X or C
Class 0	3	3	1
Class I	14	14	2
Class II <sup>a</sup>	22	12	1
Class III <sup>b</sup>	28	13	1

NOTE.—Based on Lada et al. (2006) and Muench et al. (2007), refined with class 0 sources from Enoch et al. (2009).

<sup>a</sup>including SED type THICK from Lada et al. (2006), apart from sources LRL 51 and LRL 276 which are class I, see text.

<sup>b</sup>including SED types ANEMIC and STAR from Lada et al. (2006)

TABLE 4  
IC 348: DETECTIONS OF PREVIOUSLY KNOWN RADIO SOURCES

Src HH 211-	Position (J2000)	$S_X$ (Avila et al. 2001)	$S_X$ (this work)
VLA 1	03 43 47.58 +31 59 41.45	0.14 mJy	< 0.07 mJy ( $5\sigma$ )
VLA 2	03 43 56.80 +32 00 50.41	0.09 mJy	$0.040 \pm 0.016$ mJy
VLA 3	03 43 57.60 +32 01 37.52	0.41 mJy	$0.542 \pm 0.015$ mJy
VLA 4	03 44 12.10 +31 58 29.32	0.59 mJy	< 0.08 mJy ( $5\sigma$ )

NOTE.—The source positions are from Avila et al. (2001) but have been converted to J2000.

TABLE 5  
IC 348: RADIO DETECTIONS BY EPOCH

no.	Pos	ID, RA/Dec	Epochs 1&2 $S_X$ (mJy)	$S_C$ (mJy)	$\alpha$
3	2	LRL 49 (STAR)	Ep 1: $0.829 \pm 0.025$	$0.726 \pm 0.022$	$0.24 \pm 0.11$
			Ep 2: $0.364 \pm 0.024$	$0.417 \pm 0.019$	$-0.25 \pm 0.20$
6	1	LRL 52590 (I)	Ep 1: $1.472 \pm 0.033$	$1.257 \pm 0.028$	$0.29 \pm 0.08$
			Ep 2: $1.199 \pm 0.030$	$1.095 \pm 0.023$	$0.17 \pm 0.08$
-	1	3:44:19.797 +31:59:18.63 (LRL 1888, III)	Ep 1: < 0.106 ( $5\sigma$ )	< 0.127 ( $5\sigma$ )	-
-	2	3:44:03.652 +32:05:20.67	Ep 1: < 0.080 ( $5\sigma$ )	$0.179 \pm 0.031$	-
			Ep 2: < 0.097 ( $5\sigma$ )	< 0.080 ( $5\sigma$ )	-

NOTE.—Source numbers refer to Table 2. The spectral index is only given when the corresponding error is  $\leq 0.2$ .



the field of view of both clusters. Above the respective  $5\sigma$  detection limits, we can expect about one extragalactic source in each X-band primary beam area and about three extragalactic sources in each C-band primary beam area (Windhorst et al. 1993). The probability of a chance alignment of a known YSO in the manual search with an extragalactic source is, however, exceedingly low.

Out of 19 sources, ten can be identified with YSOs from Gutermuth et al. (2008). One additional source, VLA 2a/b, has a millimeter counterpart has been described by Chandler & Richer (2000) and Chen et al. (2009) as a class 0 protostar, but it is an unresolved binary in our data. The source does not appear to have a mid-infrared (*Spitzer*-IRAC) counterpart and was not reported by Gutermuth et al. (2008). Two of these YSOs have clearly negative spectral indices, the unresolved source VLA 2a/b and [GMM2008] 97. Source 10, while not selected as a *Spitzer* YSO, has been described as an M2.7 dwarf star by Wilking et al. (2004). Stokes-*V* maps show that none of the NGC 1333 sources reported here have significant circular polarization.

Previously, Rodríguez et al. (1997) reported results from a comparable VLA observation of the region, resulting in the detection of sources VLA 1–4, all of which we can confirm, although the flux densities appear to have changed (Table 7). Additionally, these detections can be compared to the deep radio study of the region by Rodríguez et al. (1999). Their map is twice as deep as ours, with an rms noise of  $10 \mu\text{Jy}$ , and they detect 35 sources above a significance of  $5 \sigma$ . These sources include 16 X-band detections above 0.10 mJy, corresponding to the  $5\sigma$  cutoff used in our data. All but one of these sources are in the primary beam area (FWHM) of our southern pointing, but many remain undetected. However, Rodríguez et al. (1999) use a concatenated dataset consisting of several VLA observations in different configurations, requiring the use a common subset in the *uv* plane so that the beam size is  $\sim 5''$ , emphasizing more extended structures than our setup. We have searched all 20 X-band detections reported by Rodríguez et al. (1999) for counterparts in our X-band data, and we find five additional radio sources that did not make our SNR cutoff; see Table 7 where we also compare the flux densities to the values given by Rodríguez et al. (1997, 1999).

Only one source has a flux density that is statistically compatible with the previously reported value (within  $1\sigma$ ).

Finally, we report the radio detections of the different YSO evolutionary classes in Table 8. The table lists the YSOs located in the primary beam areas and the detection counts. The resulting detection fractions are again low, if marginally higher than in IC 348. Across classes 0–II, 13% of the YSOs located in the C-band primary beam areas have been detected in either radio band.

We have again checked for source variability by separately imaging the two epochs. Only two sources are detected above a significance of  $5\sigma$  in the two individual epochs, and they are listed in Table 9. Both sources, VLA 2a/b and [GMM2008] 97 show some variability and have consistently negative spectral indices.

### 3.1.3. Summary

Between the two clusters IC 348 and NGC 1333, we report the detections of radio counterparts toward 16 YSOs, 11 of these are located in NGC 1333. None of these could be unambiguously identified as nonthermal radio sources due to polarization. Using simultaneously measured negative radio spectral indices and variability instead as proxies for nonthermal emission yields two nonthermal radio counterparts in NGC 1333 (VLA 2a/b and [GMM2008] 97). Vice versa, only a single source, the class I source LRL 52590, clearly appears to be a thermal source when judged by its radio spectral index of  $\alpha = 0.25 \pm 0.06$ .

## 3.2. X-ray data

The *Chandra* X-ray observations cover a considerably larger area than the VLA observations. In the following, we mainly focus on the *Chandra* X-ray data covering the VLA primary beam areas.

### 3.2.1. IC 348

In order to reduce and process the X-ray data, we have used the ANCHORS pipeline. Briefly, the two observations are combined for the purpose of detecting point sources. Two iterations with the *ciao* wavelet-based tool *wavdetect* were performed. The first pass took a square region  $15'$  on each side and centered at the aimpoint at full resolution. The second pass examined a larger ( $25' \times 25'$ ) area

TABLE 6  
NGC 1333: RADIO DETECTIONS

no.	N/S	RA, Dec (J2000.0)	$S_X$ (mJy)	$S_C$ (mJy)	$\alpha$ (X-C)	ID (lit.)
8	S	3:28:57.382 +31:14:15.79	$< 0.11$ ( $5\sigma$ )	$0.164 \pm 0.025$		[G08] 3 (I*)
9	S	3:28:57.650 +31:15:31.33	$0.307 \pm 0.026$	$0.483 \pm 0.023$	$-0.83 \pm 0.24$	VLA 1, extragal.
10	S	3:29:00.253 +31:13:39.19	$0.170 \pm 0.037$	$< 0.14$ ( $5\sigma$ )		VLA 13, (M2.7 <sup>a</sup> )
11	S	3:29:01.964 +31:15:38.04	$1.073 \pm 0.021$	$1.237 \pm 0.021$	$-0.26 \pm 0.07$	VLA 2a/b, MMS 3 (0)
12	S	3:29:01.970 +31:15:36.22	$0.093 \pm 0.021$	$0.185 \pm 0.022$		
13	S	3:29:03.082 +31:15:51.66	$0.078 \pm 0.020$	$< 0.12$ ( $5\sigma$ )		VLA 17
14	S	3:29:03.372 +31:16:01.60	$0.100 \pm 0.021$	$0.122 \pm 0.021$		VLA 3
15	S	3:29:03.756 +31:16:03.88	$0.164 \pm 0.020$	$0.107 \pm 0.025$		VLA 4, [G08] 29 (I)
16	S	3:29:05.742 +31:16:39.71	$0.077 \pm 0.021$	$< 0.11$ ( $5\sigma$ )		VLA 22, [G08] 84 (II)
17	N	3:29:07.772 +31:21:57.03	$0.130 \pm 0.019$	$< 0.12$ ( $5\sigma$ )		[G08] 31 (I)
18	N	3:29:10.373 +31:21:58.94	$0.442 \pm 0.020$	$0.573 \pm 0.022$	$-0.48 \pm 0.15$	[G08] 97 (II)
19	S	3:29:10.420 +31:13:32.09	$0.179 \pm 0.041$	$< 0.13$ ( $5\sigma$ )		VLA 25, [G08] 6 (0 <sup>b</sup> )
20	S	3:29:11.250 +31:18:30.99	$< 0.26$ ( $5\sigma$ )	$0.171 \pm 0.028$		[G08] 7 (0 <sup>b</sup> )
21	N	3:29:17.678 +31:22:45.49	$0.055 \pm 0.018$	$0.077 \pm 0.022$		[G08] 111 (II)
22	S	3:29:20.643 +31:15:49.59	out of pb	$0.816 \pm 0.029$	–	VLA 32, extragal.
23	S	3:29:20.908 +31:15:49.36	out of pb	$0.169 \pm 0.029$	–	
24	N	3:29:21.328 +31:23:46.20	$< 0.14$ ( $5\sigma$ )	$0.089 \pm 0.024$		[G08] 117 (II)
25	S	3:29:22.266 +31:13:54.40	$< 0.77$ ( $5\sigma$ )	$0.178 \pm 0.036$		[G08] 38 (I)
26	N	3:29:30.923 +31:22:11.82	out of pb	$0.479 \pm 0.033$	–	

NOTE.—Running number continued from Table 2. The second column refers to a detection in either the northern (N) or the southern (S) pointing. The spectral index is only given when the corresponding error is  $\leq 0.3$ . [GMM2008] in ID column abbreviated to [G08]; the VLA designations are from Rodríguez et al. (1997, 1999). For the evolutionary state of source 11, see Chandler & Richer (2000); Chen et al. (2009).

<sup>a</sup>from Wilking et al. (2004).

<sup>b</sup>from Enoch et al. (2009).

TABLE 7  
NGC 1333: DETECTIONS OF PREVIOUSLY KNOWN X-BAND RADIO SOURCES

Src	Position (J2000)	$S_X(\text{total})$ (mJy) <sup>a</sup>	$S_X(\text{peak})$ (mJy, this work)	$S_C(\text{total})$ (mJy) <sup>a</sup>	$S_C(\text{peak})$ (mJy, this work)
VLA 1	03:28:57.65 +31:15:31.5	0.52	$0.307 \pm 0.026$	1.05	$0.483 \pm 0.023$
VLA 2a	03:29:01.95 +31:15:38.3	1.43	$1.073 \pm 0.021$	1.36	$1.237 \pm 0.021$
VLA 3	03:29:03.37 +31:16:01.9	0.27	$0.100 \pm 0.022$	0.12	$0.122 \pm 0.021$
VLA 4	03:29:03.75 +31:16:04.1	0.32	$0.164 \pm 0.020$	0.21	$0.107 \pm 0.025$
VLA 13	03:29:00.29 +31:13:38.6	0.13	$0.170 \pm 0.037$	< 0.06	< 0.14 ( $5\sigma$ )
VLA 17	03:29:03.08 +31:15:52.5	0.08	$0.078 \pm 0.020$	< 0.04	< 0.12 ( $5\sigma$ )
VLA 22	03:29:05.74 +31:16:39.5	0.17	$0.073 \pm 0.020$	0.17	< 0.11 ( $5\sigma$ )
VLA 25	03:29:10.46 +31:13:32.1	0.49	$0.179 \pm 0.041$	0.36	< 0.13 ( $5\sigma$ )
VLA 32	03:29:20.67 +31:15:49.6	2.55	out of pb	3.64	$0.816 \pm 0.029$

NOTE.—The source positions are from Rodríguez et al. (1997) and Rodríguez et al. (1999) but have been converted to J2000. Note that the flux densities from (Rodríguez et al. 1999) are total fluxes while we quote peak flux densities. Flux densities have been corrected for primary beam attenuation.

<sup>a</sup>from Rodríguez et al. (1997, 1999), flux density errors are listed there

TABLE 8  
NGC 1333: RADIO – DETECTED MEMBERS

	FOV (C)	FOV (X)	det.
Class 0	9	5	3
Class I	20	8	4
Class II	57	21	4
Class II/III	2	1	0

NOTE.—YSOs from Gutermuth et al. (2008), refined with class 0 sources from Enoch et al. (2009).

TABLE 9  
NGC 1333: RADIO DETECTIONS BY EPOCH

no.	Pos	ID	$S_X$ (mJy)	$S_C$ (mJy)	$\alpha$
11	S	VLA 2a/b	Ep 1: $1.216 \pm 0.034$	$1.228 \pm 0.030$	$-0.02 \pm 0.10$
			Ep 2: $1.021 \pm 0.026$	$1.236 \pm 0.026$	$-0.35 \pm 0.09$
18	N	[GMM2008] 97 (II)	Ep 1: $0.613 \pm 0.034$	$0.699 \pm 0.030$	$-0.24 \pm 0.18$
			Ep 2: $0.336 \pm 0.024$	$0.450 \pm 0.026$	$-0.54 \pm 0.24$

including all six ACIS chips with pixels binned by two. To measure source parameters, the two observations were analyzed separately. For the extraction regions of each source, the parameters of the ellipse-shaped point-spread function are interpolated from a lookup table (Allen et al. 2004) for a 95% encircled energy radius. The total counts are then scaled to 100%.

In the combined dataset, 149 sources were identified. In the two single datasets, 134 sources and 109 X-ray sources were found in datasets 8933 and 8944, respectively. The field of view of the *Chandra* observations covers 60 YSOs listed in Lada et al. (2006, Table 2), and also 30 YSOs listed in Muench et al. (2007, Tables 1, 2, and 11). Out of this total of 90 YSOs, including 5 candidate class III sources, 33 sources have X-ray counterparts within a search radius of 2". Table 10 lists the statistics of X-ray detections as a functions of object types, concatenated into totals for the different YSO classes. The table also contains information on the detection statistics for the nominal primary beam areas of the VLA observations.

The X-ray detection fraction for the YSOs is  $\sim 1/3$  in object classes I–III. None of the class 0 sources were detected in X-rays. Table 11 lists the X-ray sources with counterparts in the YSO samples. Listed are the positional difference of the X-ray detections compared to the sample, IDs, X-ray counts in both observations and information on variability, spectral and SED types. Apart from the 33 above-mentioned sources, the table lists two additional stellar sources listed by Lada et al. (2006) without an evolutionary class. LRL 1916, a class I source, shows the most spectacular variability between the two observations. The source is detected at 75 counts in the first observation, then drops to a nominal single count in the second observation.

### 3.2.2. NGC 1333

The data reduction of the NGC 1333 X-ray data is described by Winston et al. (2010). These authors find X-ray counterparts to 54 previously known YSOs and identify 41 additional X-ray sources with infrared counterparts as diskless class III YSOs. The field of view of the *Chandra* observations covers 123 out of 137 candidate YSOs listed by Gutermuth et al. (2008). As discussed by Winston et al. (2010), roughly a third

of the class I and flat-spectrum protostars and half of the class II sources are detected in X-rays. Again, none of the class 0 sources have X-ray counterparts.

## 4. Discussion

### 4.1. Combined X-ray and radio properties

The combination of the X-ray and radio data has been performed with a search radius of 1". Using larger search radii up to 4" did not increase the number of sources detected in both bands. In total, eight YSOs have been detected in both bands, four in each cluster. The X-ray fit results from ANCHORS, assuming an absorbed single-temperature APEC plasma, as well as X-ray and radio luminosities for these sources are shown in Table 13. The X-ray and radio source positions coincide within the errors.

While the VLA and *Chandra* have similar angular resolution, the existence of multiple sources within a scale of about 1" cannot be constrained from such data. Multiplicity could be due to both actual multiple stellar systems and a single object with distinct jet components. As a result, a perceived mismatch of X-ray and radio properties could be due to an unresolved multiple source.

Using the X-ray spectral parameters to predict the level of optically thin thermal free-free radio emission returns predicted flux densities that are up to 10,000 times less than what is observed. Other than these sources, several more are detected in just one of the two bands, but the overwhelming majority of *Spitzer*-selected YSOs are neither detected in X-rays, nor in centimetric radio emission.

In the following, we will separately assess the radio and X-ray detection fractions for class I and class II YSOs in the two clusters. For the sake of this discussion, we will leave out the class III sources since they are less completely catalogued in both clusters. In order to obtain a comparison between these detection fractions, we only take into account sources in the VLA primary beam (FWHM) areas. As shown in Table 14, separately for IC 348 and NGC 1333, the detection fractions are very diverse. Note that some of the fractions are based on very low numbers and thus are quite uncertain. The radio detection fractions decline with evolutionary stage, similarly in both clusters,

TABLE 10  
IC 348: X-RAY – DETECTED YSOs

	in FOV-CXO	w/X-ray	also in FOV-VLA(C)	w/X-ray
Class 0	3	0	3	0
Class I	15	7	14	5
Class II	29	10	21	5
Class III	37	16	24	10

but no such trend is apparent in the X-ray detection fractions. The X-ray detection fractions of class I and II YSOs are up to ten times higher than the radio detection fractions, but there is also the curious case of class I protostars in NGC 1333 for which the radio and X-ray detection fractions are similar, but nevertheless due to almost completely distinct sets of sources. Only a minor fraction of YSOs is detected in both bands. The present results thus do not require a tight connection between the observed X-ray and radio emission.

Compared to the range expected by the GB relation, the X-ray data are much more sensitive than the radio data, placing any radio detection with an X-ray upper limit off the Güdel-Benz relation by several orders of magnitude. For these data points, it is important to keep in mind that the observations in the two bands were carried out simultaneously so that variability cannot explain this discrepancy. While some of the YSOs with radio counterparts and X-ray upper limits are close to the radio detection limit and may be chance alignments (see above), there are also some clearly detected radio sources among the YSOs that do not have X-ray counterparts. The most striking example is the class 0 protostar source 11 in NGC 1333 with a radio flux density corresponding to a luminosity of  $L_R = 7.0 \times 10^{16} \text{ erg s}^{-1}$  but no X-ray detection. While here, any X-ray emission is likely extincted, the fact that this source is entirely incompatible with the GB relation may also point to a different radio emission mechanism, even though source 11 is among our candidate nonthermal sources due to its negative spectral index.

Since this comparison is limited by the sensitivity of the radio data presented here, it is too early to draw conclusions concerning the radio

populations of the two clusters. However, we can compare our result to previously published observations. Applying the  $5\sigma$  sensitivity limit of the present study to the results on CrA, as reported in the deep radio observations reported in Forbrich et al. (2006) and scaling to the distance of Perseus, shows that about half of the radio sources there would still be detected. While it thus seems likely that a genuine lack of radio activity plays a role in the low detection rate, the numbers involved are too low to warrant a firm conclusion.

Leaving aside the issue of non-detections in one of the two bands, we can compare the YSOs that were detected in both bands with corresponding sources from previous experiments. In spite of the fact that we do not know the dominating emission mechanism for most sources, it is also interesting to compare these YSOs to the empirical GB relation. Figure 2 shows all such sources from IC 348, NGC 1333,  $\rho$  Oph, CrA, and LkH $\alpha$  101 (Gagné et al. 2004; Forbrich et al. 2007; Osten & Wolk 2009), again relative to the GB relation. Also, we conservatively exclude sources with radio detection significance levels of  $< 5\sigma$  or less than 100 X-ray counts. Note that since the radio luminosities do not depend on a spectral fit, they are dominated by the measurement error. The X-ray luminosities, in contrast, can have uncertainties of order unity. Two things become apparent in this plot: 1) Compared to the GB relation, the YSOs appear to have higher radio luminosities for a given X-ray luminosity, and 2) there are no clear trends with evolutionary stage. About half of the sources are compatible with the GB relation even though there are sources that lie considerably below the GB relation, outside of its approximate bounds of plus or minus one order of

TABLE 11  
IC 348: X-RAY-DETECTED YSOs

LRL	RA ( <i>Chandra</i> )	Dec (J2000.0)	Offset ( $''$ )	X-ray cnts. (8933,raw)	X-ray cnts. (8944,raw)	cnt. ratio	SpT	SED type (IRAC)
1840	03:43:19.91	+32:02:43.13	1.75	33	24	1.4		III
273	03:43:52.01	+32:03:40.45	1.11	20	16	1.3		III
124	03:43:54.65	+32:00:29.96	0.24	27	42	1.6	M4.25	STAR
26	03:43:56.06	+32:02:13.35	0.37	19	12	1.6	K7	THICK
49	03:43:57.62	+32:01:37.47	0.33	56	57	1.0	M0.5	STAR
13	03:43:59.67	+32:01:54.10	0.38	182	107	1.7	M0.5	THICK
160	03:44:02.62	+32:01:35.06	0.37	29	21	1.4	M4.75	STAR
54460	03:44:02.66	+32:01:59.35	0.54	4	11	2.8		I
22021	03:44:03.64	+32:02:33.25	0.31	23	17	1.4	M5	
1916	03:44:05.79	+32:00:28.55	0.14	75	1	75.0		I
214	03:44:07.54	+32:04:08.65	0.39	10	17	1.7	M4.75	THICK
276	03:44:09.22	+32:02:38.14	0.36	15	13	1.2	M0	THICK <sup>a</sup>
173	03:44:10.23	+32:04:05.53	1.62	6	18	3.0	M5.75	THICK
105	03:44:11.30	+32:06:12.31	0.57	112	83	1.3	M0	STAR
51	03:44:13.00	+32:01:35.51	0.43	14	31	2.2		THICK <sup>a</sup>
54519	03:44:13.78	+31:55:34.85	0.47	92	86	1.1		III
31	03:44:18.21	+32:04:57.26	0.65	219	136	1.6	G1	ANEMIC
99	03:44:19.33	+32:07:34.11	1.12	105	171	1.6	M3.75	THICK
1888	03:44:19.78	+31:59:19.05	0.05	46	159	3.5		III
210	03:44:20.01	+32:06:45.49	0.15	45	47	1.0	M3.5	STAR
52590	03:44:20.43	+32:01:57.93	0.78	50	75	1.5		I
119	03:44:21.29	+32:05:02.66	0.49	91	153	1.7	M2.5	STAR
1889	03:44:21.35	+31:59:32.80	0.10	15	13	1.2		I
125	03:44:21.62	+32:06:25.71	1.07	70	171	2.4	M2.75	STAR
61	03:44:22.28	+32:05:43.23	0.54	54	80	1.5	K8	THICK
72	03:44:22.58	+32:01:53.75	0.07	81	130	1.6	M2.5	ANEMIC
30190	03:44:23.65	+32:06:47.67	0.87	158	158	1.0	M2.5	
123	03:44:24.60	+32:03:56.97	0.45	119	231	1.9	M1	STAR
97	03:44:25.58	+32:06:17.14	0.33	39	699	17.9	M2.25	THICK
5	03:44:26.05	+32:04:30.18	0.37	756	527	1.4	G8	THICK
62	03:44:26.68	+32:03:58.52	0.70	103	96	1.1	M4.75	STAR
69	03:44:27.05	+32:04:43.58	0.43	620	471	1.3	M1	STAR
68	03:44:28.49	+31:59:54.52	0.49	10	18	1.8	M3.5	THICK
55	03:44:31.40	+32:00:14.16	0.79	60	153	2.6	M0.5	THICK
52648	03:44:34.44	+31:58:00.46	1.05	50	41	1.2		I

NOTE.—Spectral types and classification information are from Lada et al. (2006) and Muench et al. (2007).

<sup>a</sup>class I, see text

TABLE 12  
NGC 1333: X-RAY – DETECTED CLASS 0–II YSOs IN NGC 1333

	in FOV-CXO	w/X-ray	also in FOV-VLA(C)	w/X-ray
Class 0	7	0	7	0
Class I	26	6	21	5
Class II	83	44	74	38

NOTE.—X-ray data from Winston et al. (2010).

TABLE 13  
YSOs DETECTED IN BOTH THE X-RAY AND THE RADIO RANGE

Source	Class	raw cnts. (total)	$n(\text{H})$ ( $10^{22} \text{ cm}^{-2}$ )	$kT$ (keV)	$L_X$ erg s $^{-1}$	$L_R(\text{X-band}^{\text{a}})$ erg s $^{-1} \text{ Hz}^{-1}$
LRL 51	I	45	–	–	–	$8.6 \times 10^{15}$
[GMM2008] 31	I	56	–	–	–	$4.3 \times 10^{15}$
LRL 52590	I	125	$1.87 \pm 0.30$	$9.21 \pm 2.10$	$4.4 \times 10^{29}$	$1.1 \times 10^{17}$
LRL 13	II	289	$1.42 \pm 0.25$	$2.20 \pm 0.47$	$8.4 \times 10^{29}$	$6.5 \times 10^{15}$
[GMM2008] 84	II	455	$1.36 \pm 0.15$	$3.40 \pm 0.56$	$7.4 \times 10^{29}$	$5.1 \times 10^{15}$
[GMM2008] 97	II	3796	$1.03 \pm 0.04$	$1.97 \pm 0.07$	$5.7 \times 10^{30}$	$3.1 \times 10^{16}$
[GMM2008] 111	II	6397	$0.28 \pm 0.01$	$2.46 \pm 0.08$	$5.0 \times 10^{30}$	$3.6 \times 10^{15}$
LRL 49	III	113	$1.02 \pm 0.24$	$2.44 \pm 0.72$	$2.9 \times 10^{29}$	$4.5 \times 10^{16}$

NOTE.—X-ray information is from ANCHORS for an energy range of 0.3–8.0 keV, spectral fits are only shown for sources with more than 100 counts.

<sup>a</sup>C band for LRL 13

TABLE 14  
COMBINED RADIO-X-RAY DETECTION STATISTICS (IC 348+NGC 1333)

Cluster	FOV (C)	X-ray	radio <sup>a</sup>	radio(X or C) & X-ray
Class 0 IC 348	3	0 (0%)	1 (33%)	0 (0%)
Class I IC 348	14	5 (36%)	2 (14%)	2 (14%)
Class II IC 348	21	5 (24%)	1 (5%)	1 (5%)
Class 0 NGC 1333	8	0 (0%)	3 (38%)	0 (0%)
Class I NGC 1333	20	5 (25%)	4 (20%)	1 (5%)
Class II NGC 1333	66	38 (58%)	4 (6%)	3 (5%)

<sup>a</sup>In C-band primary beam area.

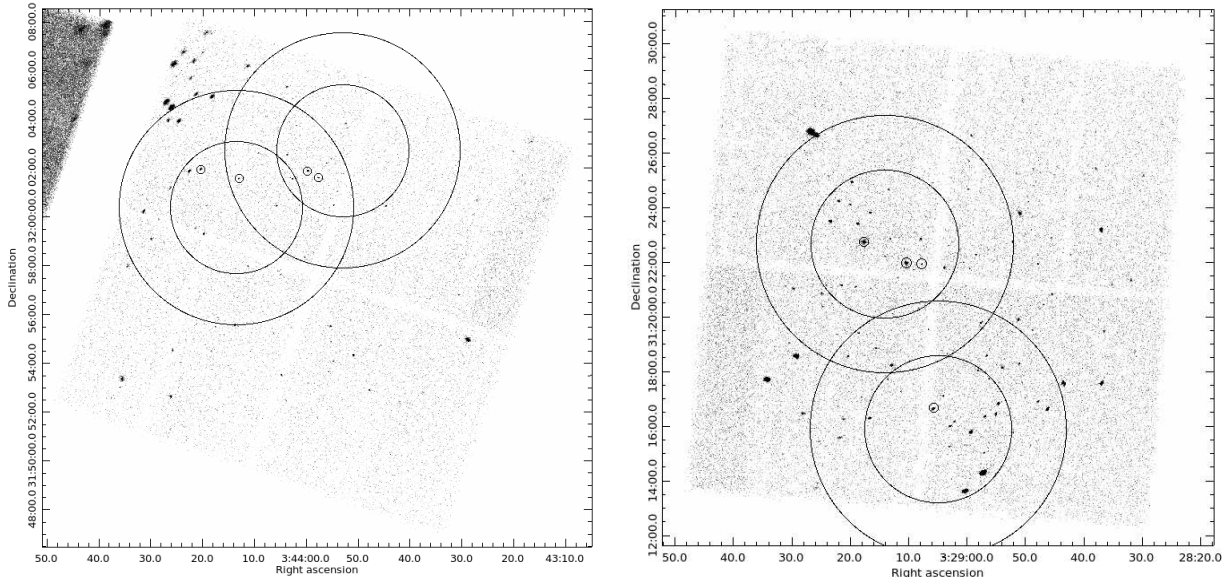


Fig. 1.— Merged *Chandra* pointings toward IC 348 (left panel) and NGC 1333 (right panel). The eastern and western pointings in IC 348 are positions 1 and 2, respectively, and the northern and southern pointings in NGC 1333 are positions N and S. The large circles indicate the primary beam sizes for the VLA pointings, the C band having a larger primary beam than the X band. YSOs detected in both bands (from Table 13) are marked by small circles.

magnitude. These sources are of all three evolutionary classes. Since all of these data points are due to simultaneous observations, variability plays only a minor role. Also, there are no clear trends concerning the type of emission and compatibility with the GB relation. For example, the thermal source LRL 52590 is the source that is least compatible with the GB relation in Figure 2. However, also note the opposite example of source 11 above. These differences may indicate different radio emission mechanisms.

In order to judge the significance of this result for YSOs in general it is important to keep in mind that this plot contains only a minor fraction of the YSOs that have been covered in the simultaneous X-ray and radio experiments. While many of the sources plotted appear radio bright, many other sources remain undetected. The detections are due to sources with extreme radio and X-ray luminosities, even though they do not represent all sources in this luminosity range. To illustrate this point, we can use the GB relation to determine the X-ray luminosity that corresponds to the approximate  $5\sigma$  radio detection limit for IC 348 and

NGC 1333,  $L_X \sim 6 \times 10^{30} \text{ ergs}^{-1}$ . This X-ray luminosity limit would include the X-ray brightest  $\sim 25\%$  G and K pre-main sequence stars in Orion (Preibisch & Feigelson 2005). None of the X-ray detected YSOs in NGC 1333 and IC 348 actually reach this luminosity. It is, however, noteworthy that six infrared-identified YSOs in NGC 1333 (from Gutermuth et al. 2008) have X-ray luminosities up to one order of magnitude below this number and lie within the VLA primary beam areas, but they do not have radio counterparts. A similar trend can be seen in the data presented by Gagné et al. (2004). There, in  $\rho$  Oph, 26 X-ray sources are more luminous than the expectation for the lower limit of the GB relation at the  $5\sigma$  radio detection limit. Of these X-ray sources, only 5 have radio counterparts. Given the radio sensitivity limits of the various studies, as shown in Figure 2, sources that are undetected in the radio range could, however, well be compatible with the GB relation at lower luminosities.

A shift toward higher radio luminosities for given X-ray luminosities had already been noted by Güdel & Benz (1993) who found that the most



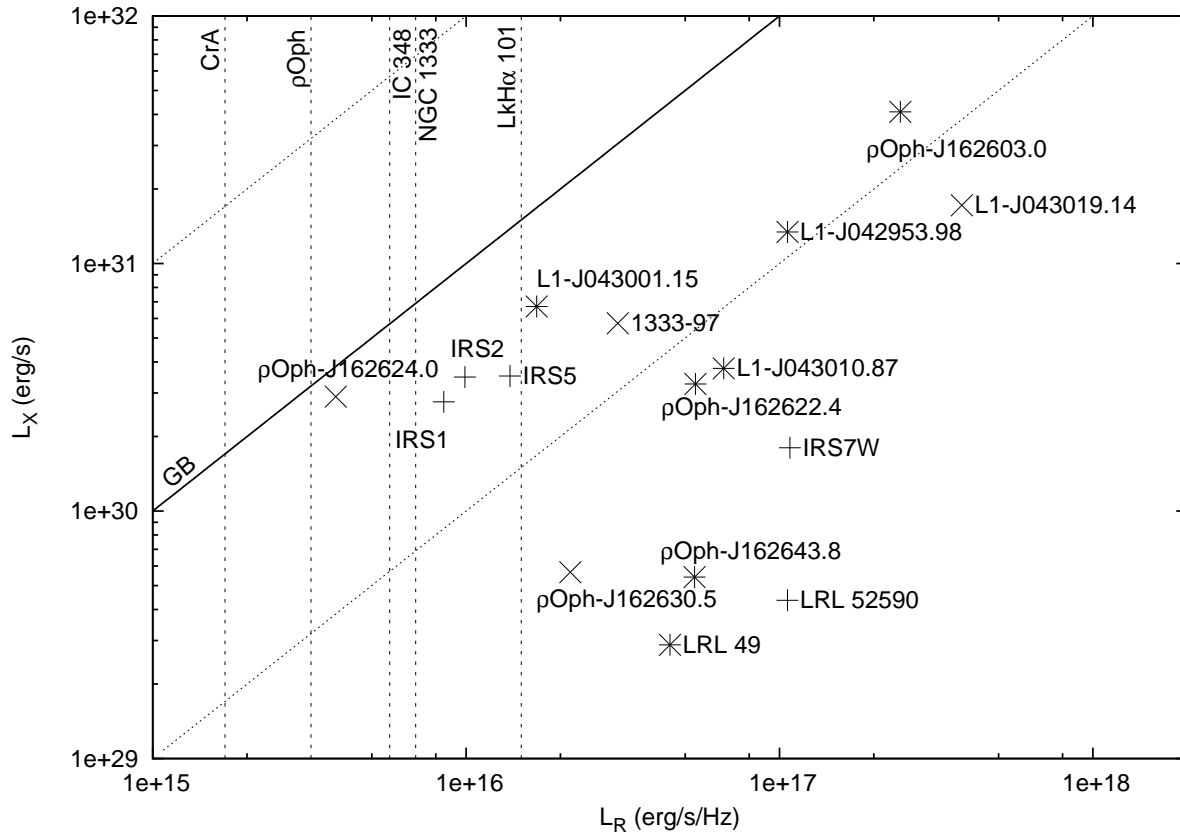


Fig. 2.— Plot of the X-ray and radio luminosities of all YSOs that have been simultaneously detected in both the X-ray and radio ranges by *Chandra* and the VLA, excluding sources with a radio detection significance of  $< 5\sigma$  and less than 100 counts in X-rays. The symbols ‘+’, ‘x’, and ‘\*’ indicate YSO classes I, II, and III, respectively. Apart from sources reported in this paper, and sources in  $\rho$  Oph from Gagné et al. (2004), scaled to a distance of 130 pc, IRS sources are in CrA (Forbrich et al. 2007), and L1 stands for LkH $\alpha$  101 (Osten & Wolk 2009). The central line marked “GB” indicates the Güdel-Benz relation with its upper and lower bounds, as reported by Güdel (2002), shown as dashed lines. The vertical lines indicate the  $5\sigma$  sensitivities of the different observations, as converted into radio luminosities at the respective distances. The limits are strictly for the simultaneous observations only (some regions have deeper radio and/or X-ray data from separate observations). The X-ray sensitivity limits are lower than the X-ray luminosity range shown (see Table 1).

luminous sources were slightly offset toward higher radio luminosities, yet still within the quoted limits of the relation. Guedel et al. (1997) suggest that not only a high X-ray luminosity, but rather the presence of a hot plasma component is conditional for the detectability of a late-type star as a strong, nonthermal radio source. However, since we also find indications for YSOs with radio but no X-ray counterparts, this may not directly apply to YSOs. They also find that while X-ray emission saturates that does not seem to be the case for the non-thermal radio emission. Consequently, if all sources discussed here were X-ray-saturated, that could also explain an offset from the GB relation. However, it seems unlikely that this would explain the offsets shown in Figure 2 where the YSOs that are furthest off the GB relation have the lowest X-ray luminosities.

One important caveat in these comparisons to the GB relation is the nature of the radio emission for each single detection since the correlation is only valid for nonthermal emission. Among the sources reported in this paper, no source can conclusively be proven to be nonthermal due to the relatively low signal-to-noise ratios: No polarization was detected, and the error bars on the radio spectral indices also do not allow us to use them as definitive criteria. Among the class I sources in the literature, CrA-IRS 5 is known to show non-thermal radio emission (Feigelson et al. 1998). This source is compatible with the GB relation (Forbrich et al. 2006, 2007). Potentially, the outlier sources have additional or alternative thermal radio components that would shift them toward higher radio luminosities. This thermal component would, however, in some cases have to account for several orders of magnitude in luminosity. A third and again completely different possibility involves coherent emission processes which, while present on the Sun (Benz et al. 2005, 2006), have not yet been identified in YSOs.

While also the thermal X-ray emission of YSOs is known to be due to at least two different sources (coronal magnetic activity and accretion), this results primarily in different temperature components in the X-ray emission, generally of similar luminosities. For our comparison of X-ray and radio luminosities, the interpretation of X-ray luminosities should thus be more straightforward.

## 5. Summary and Conclusions

We present simultaneous X-ray and radio observations of IC 348 and NGC 1333. Only three other clusters have previously been observed in this way. In summary, our main conclusions are as follows:

- The radio detection fraction for class I and class II YSOs is generally much lower than the X-ray detection fraction, particularly for the class II sources. The radio detections are not solely a subset of the X-ray detected sources. Very few YSOs ( $\sim 5\%$ ) are detected in both bands. The percentage of such X-ray-radio detections is marginally higher for class I protostars than for class II sources.
- We find a few YSOs that are detected in only one band (X-ray or radio), even though they should be easily detectable in the other band if the GB relation is applicable to these sources. Extinction helps to explain X-ray non-detections, but whether radio non-detections of X-ray sources are due to insufficient sensitivity remains unclear.
- The currently known sample of YSOs that have been simultaneously detected in both the X-ray and radio bands (across several clusters) shows that the corresponding luminosities of only about half of these sources are within one order of magnitude of the GB relation while the other half is shifted toward higher radio luminosities for a given X-ray luminosity.
- Compared to early results on the GB relation almost 20 years ago, simultaneous X-ray and radio data are now available for several source populations, minimizing the effect of variability. Also, the X-ray properties of YSOs in particular are much better defined while there has been comparably little progress on their centimetric radio properties.
- A key uncertainty in these comparisons is the nature of the radio emission since these relatively weak radio sources cannot unambiguously be identified as nonthermal radio sources. Also the radio luminosity function for these sources is basically unknown. Radio sensitivity strongly limits the size of the

dataset which can be compared to the GB relation. With the advent of the Expanded Very Large Array, the number of YSOs with defined radio properties can be expected to increase significantly. With such observations, it will be possible to look for fainter radio sources and to determine the radio luminosity function for entire YSO populations.

Support for this work was provided by the National Aeronautics and Space Administration through Chandra Award Numbers GO6-7015X and GO8-9017X issued by the Chandra X-ray Observatory Center, which is operated by the Smithsonian Astrophysical Observatory for and on behalf of the National Aeronautics Space Administration under contract NAS8-03060. S.J.W. is supported by NASA contract NAS8-03060 (Chandra). The NRAO VLA data are from programs S7874 (NGC1333) and S9056 (IC 348).

*Facilities:* CXO (ACIS), VLA

## REFERENCES

- Allen, C., Jerius, D. H., & Gaetz, T. J. 2004, in Society of Photo-Optical Instrumentation Engineers (SPIE) Conference Series, Vol. 5165, Society of Photo-Optical Instrumentation Engineers (SPIE) Conference Series, ed. K. A. Flanagan & O. H. W. Siegmund, 423–432
- André, P. 1987, in Protostars and Molecular Clouds, ed. T. Montmerle & C. Bertout, 143
- André, P. 1996, in Astronomical Society of the Pacific Conference Series, Vol. 93, Radio Emission from the Stars and the Sun, ed. A. R. Taylor & J. M. Paredes, 273
- André, P., Ward-Thompson, D., & Barsony, M. 1993, *ApJ*, 406, 122
- Avila, R., Rodríguez, L. F., & Curiel, S. 2001, *Revista Mexicana de Astronomía y Astrofísica*, 37, 201
- Bally, J., Walawender, J., Johnstone, D., Kirk, H., & Goodman, A. 2008, *The Perseus Cloud*, ed. Reipurth, B., 308
- Benz, A. O., Grigis, P. C., Csillaghy, A., & Saint-Hilaire, P. 2005, *Sol. Phys.*, 226, 121
- Benz, A. O. & Güdel, M. 1994, *A&A*, 285, 621
- Benz, A. O., Perret, H., Saint-Hilaire, P., & Zlobec, P. 2006, *Advances in Space Research*, 38, 951
- Bower, G. C., Plambeck, R. L., Bolatto, A., et al. 2003, *ApJ*, 598, 1140
- Chandler, C. J. & Richer, J. S. 2000, *ApJ*, 530, 851
- Chen, X., Launhardt, R., & Henning, T. 2009, *ApJ*, 691, 1729
- Dulk, G. A. 1985, *ARA&A*, 23, 169
- Enoch, M. L., Evans, N. J., Sargent, A. I., & Glenn, J. 2009, *ApJ*, 692, 973
- Feigelson, E. D., Carkner, L., & Wilking, B. A. 1998, *ApJ*, 494, L215
- Feigelson, E. D. & Montmerle, T. 1999, *ARA&A*, 37, 363
- Feigelson, E. D., Welty, A. D., Imhoff, C., et al. 1994, *ApJ*, 432, 373
- Forbrich, J. & Preibisch, T. 2007, *A&A*, 475, 959
- Forbrich, J., Preibisch, T., & Menten, K. M. 2006, *A&A*, 446, 155
- Forbrich, J., Preibisch, T., Menten, K. M., et al. 2007, *A&A*, 464, 1003
- Forbrich, J., Wolk, S. J., Güdel, M., et al. 2011, in *Proceedings of Cool Stars 16*, Vol. 000, Astronomical Society of the Pacific Conference Series, ed. C. Johns-Krull, M. Browning, & Andrew West, tbd, arXiv:1012.1626
- Froebrich, D., Smith, M. D., Hodapp, K., & Eislöffel, J. 2003, *MNRAS*, 346, 163
- Gagné, M., Skinner, S. L., & Daniel, K. J. 2004, *ApJ*, 613, 393
- Getman, K. V., Feigelson, E. D., Townsley, L., et al. 2002, *ApJ*, 575, 354
- Güdel, M. 2002, *ARA&A*, 40, 217
- Güdel, M. & Benz, A. O. 1993, *ApJ*, 405, L63
- Guedel, M., Guinan, E. F., & Skinner, S. L. 1997, *ApJ*, 483, 947

- Guenther, E. W., Stelzer, B., Neuhäuser, R., et al. 2000, *A&A*, 357, 206
- Gutermuth, R. A., Myers, P. C., Megeath, S. T., et al. 2008, *ApJ*, 674, 336
- Herbst, W. 2008, *Star Formation in IC 348*, ed. Reipurth, B., 372
- Hirota, T., Bushimata, T., Choi, Y. K., et al. 2008, *PASJ*, 60, 37
- Lada, C. J. 1987, in *IAU Symposium, Vol. 115, Star Forming Regions*, ed. M. Peimbert & J. Jugaku, 1–17
- Lada, C. J., Muench, A. A., Luhman, K. L., et al. 2006, *AJ*, 131, 1574
- Lombardi, M., Lada, C. J., & Alves, J. 2010, *A&A*, 512, A67
- Muench, A. A., Lada, C. J., Luhman, K. L., Muzerolle, J., & Young, E. 2007, *AJ*, 134, 411
- Mukai, K. 1993, *Legacy*, 3, 21
- Osten, R. A. & Wolk, S. J. 2009, *ApJ*, 691, 1128
- Preibisch, T. & Feigelson, E. D. 2005, *ApJS*, 160, 390
- Rodríguez, L. F., Anglada, G., & Curiel, S. 1997, *ApJ*, 480, L125
- Rodríguez, L. F., Anglada, G., & Curiel, S. 1999, *ApJS*, 125, 427
- Shirley, Y. L., Claussen, M. J., Bourke, T. L., Young, C. H., & Blake, G. A. 2007, *ApJ*, 667, 329
- Walawender, J., Bally, J., Francesco, J. D., Jørgensen, J., & Getman, K. 2008, *NGC 1333: A Nearby Burst of Star Formation*, ed. Reipurth, B., 346
- White, S. M., Pallavicini, R., & Kundu, M. R. 1992, *A&A*, 259, 149
- Wilking, B. A., Gagné, M., & Allen, L. E. 2008, *Star Formation in the  $\rho$  Ophiuchi Molecular Cloud*, ed. Reipurth, B., 351
- Wilking, B. A., Meyer, M. R., Greene, T. P., Mikhail, A., & Carlson, G. 2004, *AJ*, 127, 1131
- Windhorst, R. A., Fomalont, E. B., Partridge, R. B., & Lowenthal, J. D. 1993, *ApJ*, 405, 498
- Winston, E., Megeath, S. T., Wolk, S. J., et al. 2010, *AJ*, 140, 266